Ruthenium Complexes with PNN Pincer Ligands Based on (Chiral) Pyrrolidines

Bootsma, Johan; Guo, Beibei; de Vries, Johannes G.; Otten, Edwin

Published in:
Organometallics

DOI:
10.1021/acs.organomet.9b00765

Publication date:
2020

ORGANOMETALLICS

pubs.acs.org/Organometallics

Article

Ruthenium Complexes with PNN Pincer Ligands Based on (Chiral) Pyrrolidines: Synthesis, Structure, and Dynamic Stereochemistry

Johan Bootsma, Beibei Guo, Johannes G. de Vries,* and Edwin Otten*

Cite This: *Organometallics* 2020, 39, 544–555

Read Online

ACCESS | Metrics & More | Article Recommendations | Supporting Information

ABSTRACT: We report the synthesis of lutidine-based PNN type metal pincer complexes, using achiral (pyrrolidine) as well as chiral ((*R*,*R*)-2,5-dimethylpyrrolidine and (*R*)-2-methylpyrrolidine) substituents at the N side arm of the pincer ligand. With the six-coordinate saturated Ru pincers (PNN)Ru(H)(CO)(Cl), which have an aromatic pyridine ligand backbone, as the starting materials, treatment with strong base (KO^{t}Bu) generated the corresponding dearomatized pincer complexes (PNN′)Ru(H)(CO). Spectroscopic, crystallographic, and computational studies demonstrate that the C-centered chirality from the chiral pyrrolidine group exerts a small but non-negligible influence on the preferred stereochemistry at Ru (and N in the case of (*R*)-2-methylpyrrolidine) that is reflected in the equilibrium distribution of diastereomers of these Ru complexes in solution. Our data show that the N- and Ru-based stereogenic centers in this class of compounds are stereochemically labile and the mechanisms for epimerization are discussed. Inversion at the Ru center in the dearomatized complexes is proposed to occur via a rearomatized Ru(0) intermediate in which the Ru-bound hydride is transferred to the ligand. Support for this comes from the spectroscopic characterization of a closely related Ru(0) species that is obtained by reaction with CO. Testing these catalysts in enantioselective oxa-Michael addition or transfer hydrogenation led to racemic products, while a low ee (8%) was observed in the hydrogenation of 4-fluoroacetophenone. The lack of appreciable enantioinduction with these catalysts is ascribed to the kinetic lability of the Ru stereocenter, which results in the formation of equilibrium mixtures in which several diastereomers of the catalyst are present.

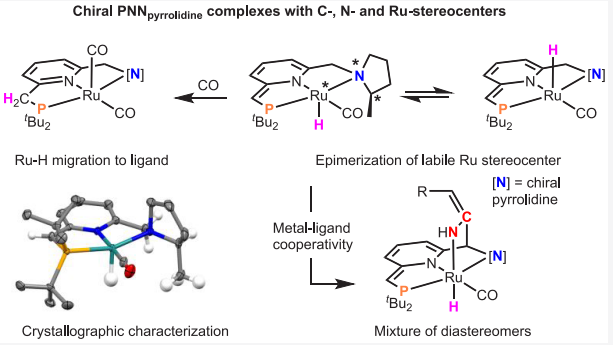

INTRODUCTION

Transition-metal complexes with pincer ligands have received widespread interest for applications in organometallic chemistry and catalysis because they allow rational tuning of steric/electronic properties around the metal center and result in compounds that have high thermal stability.[1] The ability to vary the three donor sites that bind to the metal center independently has led to a wide range of structural motifs that all lead to the characteristic meridional coordination mode of these ligands. Despite the large variation in pincer ligand designs that is possible, the study of *chiral* pincers has been limited.[2] Selected examples are shown in Chart 1 and include anionic (phenyl-based) ligands with chiral oxazoline or imidazoline substituents (**A**),[3] PCP pincer ligands bearing phosphine groups with chiral substituents (**B**, **C**)[4,5] or related amine (NCN) derivatives based on proline (**D**).[6] In addition, compounds with P-stereogenic centers (**E**)[7] or ligands with an asymmetric carbon center in the benzylic position of the pincer "arm" connecting the ligating sites (**F**)[8] have been reported. In contrast to (anionic) phenyl-based ligands, ruthenium complexes with a pincer ligand based on a central pyridine ring have been shown to lead to metal–ligand cooperation as a result of (reversible) aromatization/dearomatization sequences of the central pyridine in the ligand scaffold, which introduces a double bond to the benzylic position. This reactivity has been pioneered by the Milstein group and shown to give rise to unique catalytic applications, in particular in the area of dehydrogenative coupling of alcohols (and/or amines) to give esters or amides.[9]

We have been interested in Milstein-type Ru PNN pincer complexes in the context of nitrile reactivity and have shown that metal–ligand cooperative activation of unsaturated nitriles[10] leads to conjugate addition of alcohols to *α*,*β*-unsaturated nitriles (oxa-Michael addition).[11] Similar catalytic reactivity was also observed with the manganese analogues.[12] In addition to conjugate 1,4-additions, we recently developed 1,2-additions of H_2O to a wide range of nitriles to form the corresponding amides using Ru catalysts on the basis of metal–ligand cooperation with PNN or PNP pincer ligands.[13]

Received: November 8, 2019
Published: February 5, 2020

Chart 1. Selected Chiral Pincer Ligands

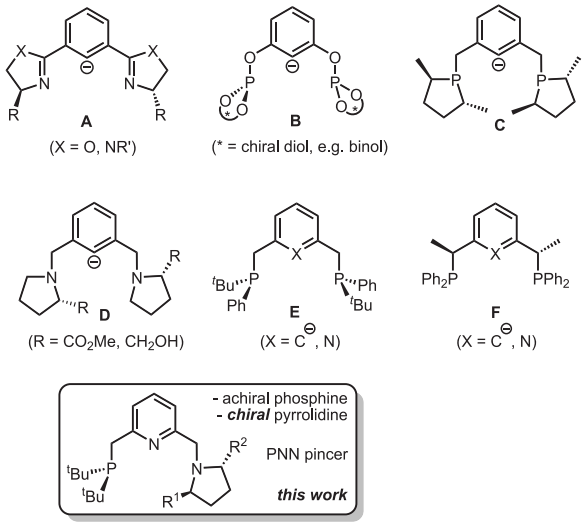

(Oxa-)Michael addition reactions to β-substituted α,β-unsaturated nitriles leads to the formation of an asymmetric carbon center, and thus it would be of interest to control the enantioselectivity of this reaction. In our previous investigation of oxa-Michael additions via metal−ligand cooperativity,[11a] the DFT-computed transition state for the addition of the alcohol nucleophile suggests that concerted alcohol deprotonation/nucleophilic attack is the key C−O bond-formation step; the calculations suggest that attack of the alkoxide preferentially occurs to the enantioface of the olefin that is most accessible (i.e., from the Ru−CO side ("front"), away from the P^{t}Bu$_2$ groups (see Scheme 1A). Thus, ligands that are able to transfer chiral information to control the stereochemistry at Ru (i.e., the position of the Ru−H relative to the square plane containing the pincer donors) could potentially lead to enantioenriched products (Scheme 1B).

Given these considerations, we were interested in exploring chiral PNN pincer ligands and decided to introduce a (chiral) pyrrolidine ring at the N arm. To the best of our knowledge, although chiral amines have been used in carbene-based pincers,[14] chiral pyrrolidine-based derivatives of Milstein's Ru PNN complexes have not been prepared. It should be noted that a series of chiral phospholane-based PNN Mn catalysts were recently described, which give high enantioselectivity in ketone hydrogenation.[15]

Here we report the synthesis of a series of (chiral) pyrrolidine-based PNN ligands and their corresponding Ru complexes. Starting from the parent (achiral) pyrrolidine, we describe PNN pincers with the C_2-symmetric (*R*,*R*)-2,5-dimethylpyrrolidine group as well as the fully asymmetric (C_1) (*R*)-2-methylpyrrolidine group. The solid-state and solution structures for these compounds were investigated by a combined experimental/computational study to provide insight into the nature of the diastereomeric products that are obtained and their relative stability.

RESULTS AND DISCUSSION

Synthesis and Characterization of PNN Ligands. The methylpyrrolidines required for the synthesis of the chiral pincer ligands can be derived from nature's chiral pool: yeast-catalyzed reduction of 2,5-hexadione provides access to (*R*,*R*)-2,5-dimethylpyrrolidine[16] (Scheme 2A), and reduction of the carboxylate group of L-proline yields (*R*)-2-methylpyrrolidine[17] (Scheme 2B).

Scheme 2. Chiral Methylpyrrolidines from Nature's Chiral Pool

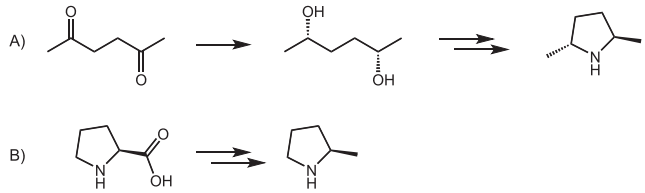

The synthesis of the (chiral) PNN ligands was accomplished by modification of the procedure reported by Milstein and co-workers,[18] via sequential installation of the amine side arm followed by the phosphine (Scheme 3). Specifically, the amine group was introduced on the lutidine backbone by alkylation of

Scheme 1. (A) Transition State for Oxa-Michael Addition[a] and (B) Stereochemistry at Ru Determining the Olefin Enantioface That Is Accessible for Nucleophilic Attack

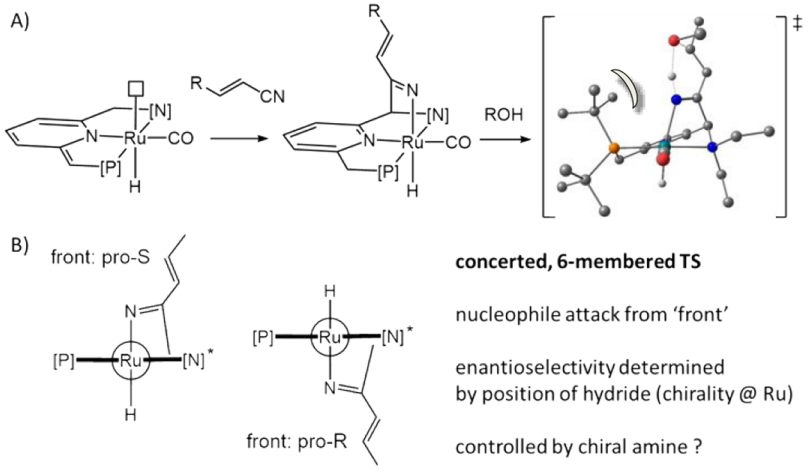

[a]The CH_3 groups of isopropyl alcohol are omitted for clarity.

https://dx.doi.org/10.1021/acs.organomet.9b00765
Organometallics 2020, 39, 544−555

Scheme 3. Synthesis of PNN ligands 4−6, either by Direct Means or via the Borane-Protected PNN·2BH$_3$

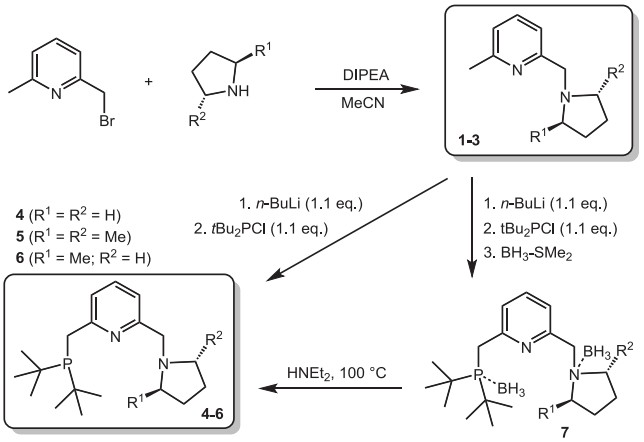

(substituted) pyrrolidine with 2-bromomethyl-6-methylpyridine. This proved to be straightforward when Hünig's base was used, providing the alkylation products **1**−**3** in isolated yields ranging from 45 to 74% (**1**, $R^1 = R^2 = H$; **2**, $R^1 = R^2 = Me$; **3**, $R^1 = Me$, $R^2 = H$). In the ^1H NMR spectra of **2** and **3**, the pyrrolidine methyl peaks were clearly distinguishable as doublets at 0.96 and 1.12 ppm for **2** and **3**, respectively. Whereas for **1** the homotopic protons of the benzyl amine fragment are observed as a singlet (3.71 ppm), the corresponding signals for **2** and **3** are diastereotopic and give rise to a pair of mutually coupled doublets at 3.83 and 3.71 ppm (J = 14.9 Hz) for **2**, and at 4.20 and 3.27 ppm (J = 13.8 Hz) for **3**.

The phosphine group was subsequently introduced by deprotonation of the remaining lutidine methyl group with *n*-butyllithium at −10 to 0 °C in diethyl ether, followed by addition of tBu$_2$PCl at −78 °C. After workup, the PNN ligands based on pyrrolidine (**4**, $R^1 = R^2 = H$), and (*R*,*R*)-2,5-dimethylpyrrolidine (**5**, $R^1 = R^2 = Me$) were obtained as light yellow oils in 68% and 40% yields, respectively. Alternatively, the ligand based on (*R*)-2-methylpyrrolidine was obtained as the air-stable BH$_3$ adduct (**7**, $R^1 = Me$, $R^2 = H$), from which the borane protecting groups could subsequently be removed by treatment with diethylamine at 100 °C for 3 days to give the free ligand **6** (36% over two steps).[19] Although the deprotection step itself was quantitative and the free PNN ligand **6** could be obtained easily from the reaction mixture, some boron-containing impurities proved difficult to remove. The presence of these minor impurities, however, did not impede the formation of metal complexes, which were isolated in analytically pure form.

Crystals of PNN·2BH$_3$ (**7**) suitable for single-crystal X-ray crystallography were obtained from a DCM/hexane solution. On the basis of a refinement of Flack's parameter[20] (x = 0.02(5)), the stereochemistry of the 2-methylpyrrolidine ring is retained during the synthesis of **7**. Furthermore, the structure shows the presence of two BH$_3$ molecules bound to P and N (Figure 1). The formation of the bis-BH$_3$ adduct **7** was also confirmed by ^{11}B NMR spectroscopy: a doublet was present at −42.39 ppm (J = 60.7 Hz), which was assigned to the P−BH$_3$ moiety, and a broad singlet at −14.96 ppm, which was assigned to the N−BH$_3$ group. The ^{31}P NMR spectrum displayed a single resonance at 44.66 ppm, which showed coupling to the boron nuclear spin. The chemical shift is similar to that of a

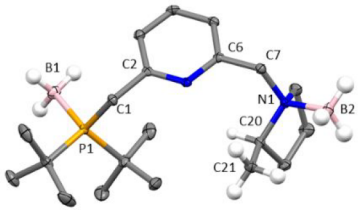

Figure 1. Molecular structure of the bis-borane adduct **7** ($R^1 = R^2$ = Me), showing 50% probability ellipsoids. All hydrogens have been omitted for clarity except for those of the borane groups, as well as those of the CH$_3$ and CH fragment of the pyrrolidine group. Selected bond lengths: N1−B2 = 1.641(2), P1−B1 = 1.928(2), C6−C7 = 1.514(2), C1−C2 = 1.510(2).

phosphine−borane adduct of a previously reported PNN ligand by de Bruin and co-workers (47.13 ppm).[19b] The identity of the free PNN ligands **4**−**6** was confirmed by NMR spectroscopy. Diagnostic resonances are observed in the ^{31}P NMR spectra at 34.6 ppm (**4**), 35.5 ppm (**5**), and 32.30 ppm (**6**), in agreement with values of previously reported (achiral) PNN ligands.[18,21]

Synthesis and Characterization of Ru PNN Complexes. Derivatives of Milstein's complex (PNN)Ru(H)(CO)(Cl) in which the NEt$_2$ group is replaced by pyrrolidine (**8**), (*R*,*R*)-2,5-dimethylpyrrolidine (**9**), and (*R*)-2-methylpyrrolidine (**10**) were synthesized by reacting the PNN ligands **4**−**6** with (Ph$_3$P)$_3$Ru(H)(CO)(Cl) in THF at 65 °C (Scheme 4).[18]

Scheme 4. Synthesis of Complexes 8−10

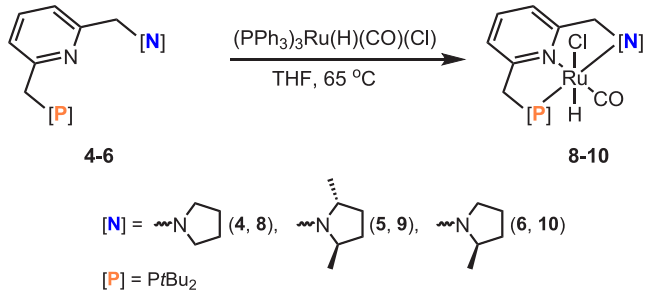

The products were isolated as yellow solids in 65−68% yield. Compound **8** with an unsubstituted pyrrolidine group showed a ^{31}P NMR resonance at 106.9 ppm and a doublet at −15.43 ppm (J = 27.3 Hz) in the ^1H NMR spectrum due to the Ru−H moiety. The dimethylpyrrolidine analogue **9** displayed two ^{31}P NMR resonances at 111.11 ppm (major) and 109.13 ppm (minor) and two upfield ^1H NMR doublets for the Ru−H fragment (major, −14.82 ppm, J = 27.1 Hz; minor, −15.19 ppm, J = 27.6 Hz). The ratio between these two species is 57:43 on the basis of integration. The observation of two distinct species in similar amounts suggests that **9** is formed as a mixture of diastereoisomers (epimers) that have comparable stability. These two epimers, which will be denoted **9a** and **9b**, differ in the orientation of the Ru−H group with respect to the ligand plane and can be assigned by reference to the clockwise/anticlockwise disposition of the "equatorial" ligands in a view along the Cl−Ru−H axis (Figure 2).[22]

The methylpyrrolidine analogue **10** showed four ^{31}P NMR resonances around 105 ppm in acetone-d_6, in a ratio of

https://dx.doi.org/10.1021/acs.organomet.9b00765
Organometallics 2020, 39, 544−555

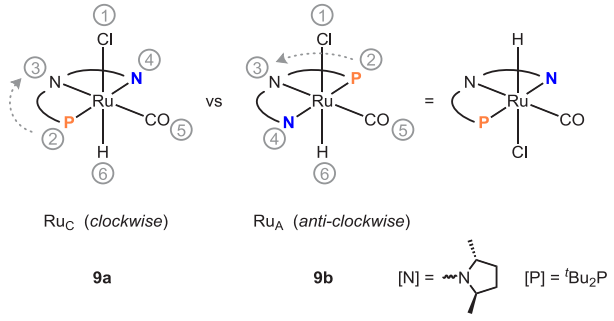

Figure 2. Descriptors clockwise (Ru_C) and anticlockwise (Ru_A) used to denote the stereochemical configuration around the Ru center in the octahedral (PNN)Ru(H)(CO)(Cl) complexes (ligand priority numbers indicated). Assignment of the stereochemistry of compounds **9a,b** is indicated.

1.00:0.97:0.48:0.33 on the basis of integration. Similarly, the ^{1}H NMR spectrum contains four doublets around −15 ppm due to the Ru−H moiety, indicating the presence of four different diastereomers. Assuming that no racemization at the asymmetric C atom in the pyrrolidine ring has taken place, these diastereomers (**10a−d**) arise from all possible combinations of the stereochemistry at the Ru and N stereogenic centers (Ru_C/Ru_A and N_S/N_R, respectively; see Figure 3).

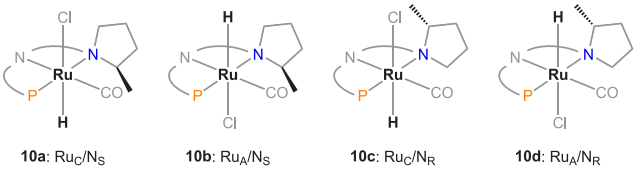

Figure 3. Simplified structure of the four diastereomers **10a−d** that arise from the Ru and N stereocenters.

Crystals of the achiral complex **8** suitable for X-ray analysis, which were obtained from a concentrated THF solution stored at −30 °C overnight, confirmed the formation of the desired ruthenium complex (see Figure 4 and pertinent metrical parameters in Table 1). In the case of the dimethylpyrrolidine complex **9**, crystals were grown from an acetone-d_6 solution stored at room temperature. This allowed one of the two diastereomers to be obtained selectively; dissolution of the crystals resulted in a single set of resonances in the ^{1}H and ^{31}P NMR spectra. No changes in the ^{1}H NMR spectrum were observed after standing for several days, indicating that isomerization (epimerization at Ru) does not occur on this

Table 1. Selected Metrical Data (Bond Distances in Å and Angles in deg) for Compounds 8, 9b, and 10a and Dearomatized Complex 13a

	8	9b	10a[a]	13a
Ru01−N1	2.259(4)	2.267(1)	2.268(3)	2.208(2)
Ru01−N2	2.118(6)	2.113(1)	2.107(3)	2.079(2)
Ru01−P1	2.274(1)	2.2626(4)	2.274(1)	2.2771(6)
Ru01−CO	1.842(7)	1.830(2)	1.835(5)	1.838(2)
N2−Ru01−CO	171.9(2)	172.38(6)	175.0(2)	176.15(9)
N2−Ru01−H1	87(3)	87.8(8)	89(2)	98(1)
Cl1−Ru01−H1	180(3)	170.8(8)	175(2)	
N1−Ru01−P1	158.1(1)	159.33(4)	159.5(1)	157.80(5)

[a]These values are for the molecule without disorder.

time scale. Comparison of the NMR spectrum of the crystalline material and that of the mixture before workup showed that the minor reaction product preferentially crystallizes from solution. A single-crystal X-ray diffraction study showed that it crystallizes in space group $P2_12_12_1$ (one of the Sohncke-type spacegroups)[23] and is present as isomer **9b** (see Figure 4 and Table 1), which is the epimer that has an anticlockwise arrangement of the PNN pincer around the ruthenium center (Ru_A).

Similarly, crystals of methylpyrrolidine complex **10** suitable for X-ray crystallography were obtained from a concentrated acetone solution at room temperature (space group $P2_1$). The asymmetric unit contains two independent molecules; both show the expected octahedral geometry around the Ru center, with the carbonyl group bound in the position trans to the pyridine-N donor. One of the independent molecules is well-defined and has little disorder, which is isomer **10a** having a clockwise (Ru_C) stereochemistry around the metal center (Figure 5, left; pertinent metrical parameters in Table 1). The other molecule in the unit cell shows some disorder in the methylpyrrolidine ring, where two possible conformations of this ring seem to be superimposed on one another. Regardless of the disorder, it is clear that the stereochemistry at Ru is inverted in this molecule (anticlockwise; Ru_A). The disorder in the pyrrolidine ring could be satisfactorily modeled with a two-site occupancy model that differed in the N stereochemistry due to rotation around the C(7)−N(1) bond and N inversion (isomers **10b,d**). Refinement of the site occupancy factors for both disorder components converged at 0.55 for the major fraction (**10d**), indicating that three out of the four diastereomers that are possible for complex **10** are present in the single crystal in the approximate ratio **10a:10b:10d** =

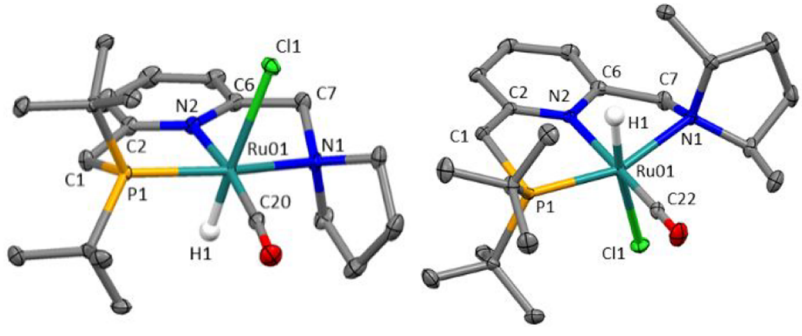

Figure 4. Molecular structures of complexes **8** (left) and **9b** (right), showing 50% probability ellipsoids. The hydrogen atoms have been omitted for clarity, except for the hydride ligand.

https://dx.doi.org/10.1021/acs.organomet.9b00765
Organometallics 2020, 39, 544−555

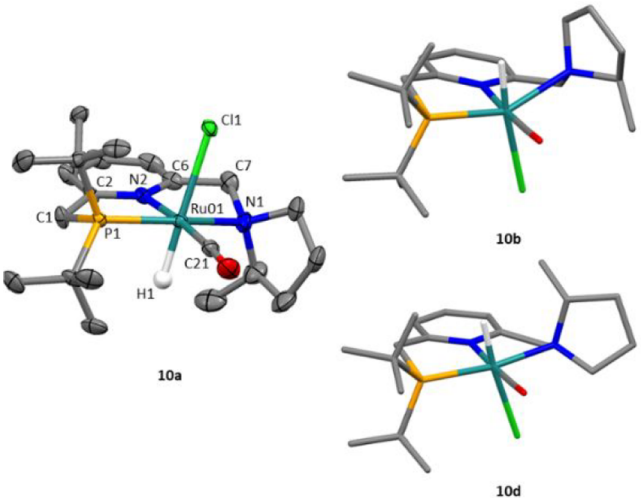

Figure 5. Molecular structures of the two independent molecules in crystals of **10**: diastereomer **10a** (left) and the disorder components **10b** (top right) and **10d** (bottom right). The structure of **10a** is shown with 50% probability ellipsoids, and the disorder components **10b,d** are shown as capped sticks. The hydrogen atoms have been omitted for clarity, except for the hydride ligand.

1:0.45:0.55. A THF-d_8 solution of the crystalline material, however, showed the presence of all four possible diastereomers in a ratio of 1.00:1.01:0.41:0.43. Although the possibility that other crystals contain different isomer ratios (including the presence of isomer **10c**) cannot be excluded, it seems likely that the appearance of **10c** in solution is due to N inversion in compound **10a**, which indicates that the amine arm is hemilabile in solution (vide infra).

Synthesis and Isomerization Behavior of Dearomatized Complexes. As described in the literature, lutidine-based (PNN)Ru(H)(CO)(Cl) complexes can be deprotonated at the benzylic phosphine side arm with concomitant loss of a chloride ion.[18] This results in formation of an exocyclic double bond and dearomatization of the pyridine in the ligand backbone. The complexes (PNN)Ru(H)(CO)(Cl) (**8**–**10**) were reacted with KO*t*Bu in THF to give the dark red complexes (PNN′)Ru(H)(CO) (PNN′ = dearomatized pincer ligand) with pyrrolidine (**11**), (*R*,*R*)-2,5-dimethylpyrolidine (**12**), and (*R*)-2-methylpyrrolidine substituents (**13**) (Scheme 5). For **11**, the ^{1}H NMR spectrum shows a Ru−H peak that is

Scheme 5. Synthesis of Dearomatized Ru Complexes 11−13

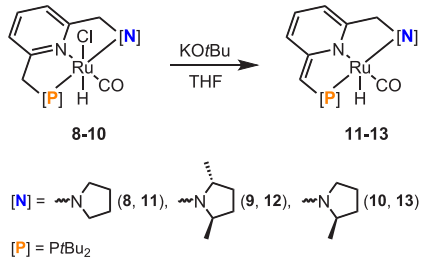

shifted ca. 10 ppm upfield to δ −25.78 ppm (J = 25.8 Hz). Resonances at δ 6.31, 6.05, and 5.26 ppm are indicative of a dearomatized pyridine pincer backbone. Compound **11** has a ^{31}P NMR resonance at δ 95.8 ppm. For the complexes with enantiomerically pure pyrrolidine groups, deprotonation resulted in similar spectral features, which indicates the formation of the corresponding dearomatized complexes **12** and **13**.

With a **9a,b** mixture as the starting material, the dearomatized product **12** was also obtained as two diastereomers, which show hydride peaks in the ^{1}H NMR spectrum at −25.62 ppm (major) and −26.81 ppm (minor). Whereas the ratio of isomers in the starting material **9** is 57:43, compound **12** is obtained as a 76:24 mixture, indicating that (partial) epimerization of the Ru−H bond has occurred. Moreover, when pure, crystalline **9b** (which does not isomerize in solution) was reacted with KO*t*Bu, the epimers **12a,b** of the dearomatized product **12** were both obtained (Scheme 6), but

Scheme 6. Ru−H Epimerization of Isomers 12a,b in Solution

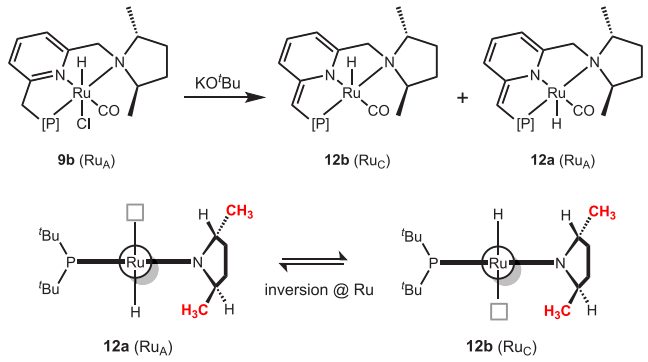

the rate at which equilibrium is established is solvent-dependent. Deprotonation of **9b** in THF solution resulted in the instantaneous formation of the equilibrium mixture (76:24 ratio). Conversely, when the reaction is carried out in benzene, the approach to equilibrium is slow, reaching a similar composition only in ca. 2 days (see Figure S1).

Analysis of the (*R*)-2-methylpyrrolidine derivative **13** by ^{1}H NMR spectroscopy indicated that two new Ru−H species had formed within 20 min, with a relative ratio of 71:29. The observation of two isomers is surprising because the precursor **10** is a mixture of four isomers. Thus, the dearomatized product **13** is stereochemically labile and rapidly establishes an equilibrium in which only two isomers are present. To investigate the identity of the two isomers of **13**, a 2D-NOESY NMR experiment was performed (see the Supporting Information for spectral data). Through-space correlations were observed between the Ru−H signal of the major isomer (−25.85 ppm) and a ^{t}Bu group (1.33 ppm) as well as the pyrrolidine methyl group (1.11 ppm). The presence of these nuclear Overhauser effects is consistent with the assignment of the major isomer as compound **13a** (Scheme 7). The hydride signal of the minor species only showed a correlation with a *t*Bu group. In addition, the pyrrolidine methyl group shows a cross peak with a different *t*Bu group, indicating these to be sufficiently proximate to experience the nuclear Overhauser effect. These observations indicate that the minor isomer has structure **13b** (Scheme 7). Apparently, diastereomers **13c,d** are thermodynamically less stable and are therefore not observed in the equilibrium mixture.

Crystals were obtained from THF/hexane at −30 °C and analyzed by X-ray diffraction (space group $P2_12_12_1$). The structure solution shows it to be isomer **13a** (see Figure 6, selected metrical parameters in Table 1). In comparison to the precursor **10a**, the Ru01−N1 (2.208(2) vs. 2.268(3) Å) and

https://dx.doi.org/10.1021/acs.organomet.9b00765
Organometallics 2020, 39, 544−555

Scheme 7. Interconversion among Isomers 13a–d in Solution

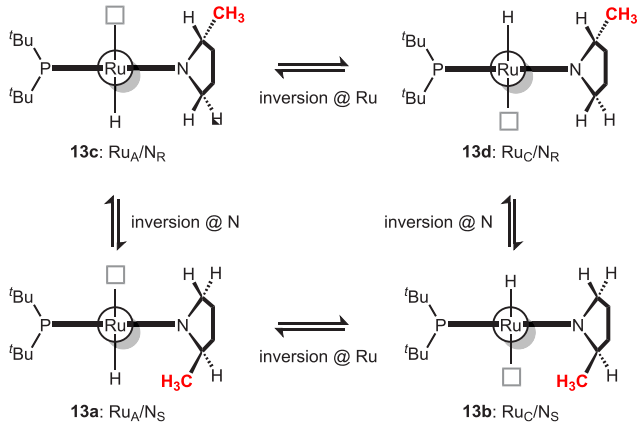

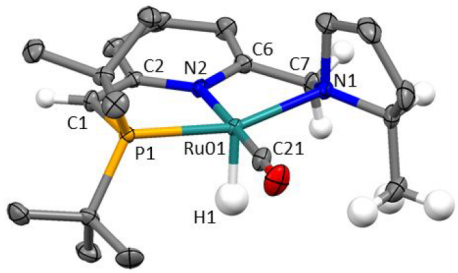

Figure 6. Crystal structure of the dearomatized complex (PNN′)Ru(H)(CO) **13a**, displayed as 50% ellipsoids.

Ru01–N2 (2.079(2) vs 2.107(3) Å) bonds have shortened, but the Ru01–P1 (2.2771(6) vs 2.274(1) Å) and Ru01–CO bonds (1.838(2) vs. 1.835(5) Å) remain virtually unchanged. A key feature of this dearomatized complex is its exocyclic double bond, which is present at the phosphine side arm of the ligand with C1–C2 = 1.371(3) Å, which is distinctly shorter than the C1–C2 bond of 1.499(5) Å in the precursor **10a**. In addition, partial P=C double bond character is indicated by a decrease in the P1–C1 distance (1.846(4) Å in **10a** vs 1.773(2) Å in **13a**). The dearomatization of the pyridine ring is evident from the localized bonding within the six-membered ring, with two short C=C (1.364(3)/1.356(3) Å) and two long C–C bonds (1.419(3)/1.443(3) Å). Similar bond length differences have been found in a related, symmetrical PNP Ru complex[24] and the Re analogue.[25] Despite the widespread use of dearomatized pyridine-based PNN Ru complexes in catalysis, the data presented here for **13a** provide the first structural characterization of such a species.

Dissolution of pure, crystalline **13a** in C_6D_6 immediately followed by NMR analysis showed that only one species is present (>95%), with resonances that match those of the major species before crystallization. Upon standing at room temperature, however, the minor isomer **13b** slowly appears, confirming that these two species are in equilibrium (Figure S2). After ca. 1 week in C_6D_6 solution, the same equilibrium ratio is obtained as in the in situ preparation. Taken together, these results show that the same two products (**13a,b**) are ultimately obtained regardless of whether one starts from an equilibrium mixture of the precursor **10a–d** or from the pure compound **13a**. Thus, interconversion among all four diastereomers of **13** is possible to result in the thermodynamic product mixture, which implies that inversion at N and at Ru both occur in solution (Scheme 7).

The **13a**:**13b** ratio of 71:29 obtained from the NMR integration at room temperature translates to a Gibbs free energy difference of 0.52 kcal/mol. This is in agreement with DFT calculations using the TPSS functional[26] and Ahlrich's def2-TZVP basis set,[27] including Grimme's dispersion correction.[28] The geometries of all four diastereomers were optimized in the gas phase, which resulted in the lowest Gibbs free energy for the major diastereomer that is observed experimentally (**13a**). Complex **13b**, resulting from epimerization at Ru, is computed to be slightly higher in energy (0.42 kcal/mol), while the other two isomers are disfavored by 2.4–2.6 kcal/mol and therefore present in too little amount to be observable by NMR spectroscopy (≤1%) at equilibrium.

Mechanism of Ru–H Epimerization. The solution NMR studies discussed above indicate that in the coordinatively saturated, aromatic (PNN)Ru(H)(CO)(Cl) complexes **8–10** inversion of stereochemistry at Ru does not occur at room temperature. In contrast, the dearomatized compounds **11–13** are dynamic in solution and are able to invert the stereochemistry at N as well as at Ru. The former (N inversion) can occur by dissociation of the (substituted) pyrrolidine followed by low-barrier pyramidal inversion of the amine.[24,29] Mechanistically, inversion of the stereochemistry at Ru (e.g., implicated in the formation of an equilibrium mixture of **13a,b** upon dissolution of pure **13a**) is less readily explained. Epimerization at Ru can be envisaged to occur by two different pathways: (i) hydride migration via the coordination site that is vacated in the pincer plane by detachment of the (hemilabile) amine donor or (ii) hydride transfer to the unsaturated arm of the pincer ligand to generate a planar, pseudo-C_s-symmetric Ru(0) intermediate (Scheme 8).

DFT calculations were carried out to probe each of these pathways using the methylpyrrolidine-substituted complex **13a**

Scheme 8. DFT-Calculated Ru–H Epimerization Pathways[a]

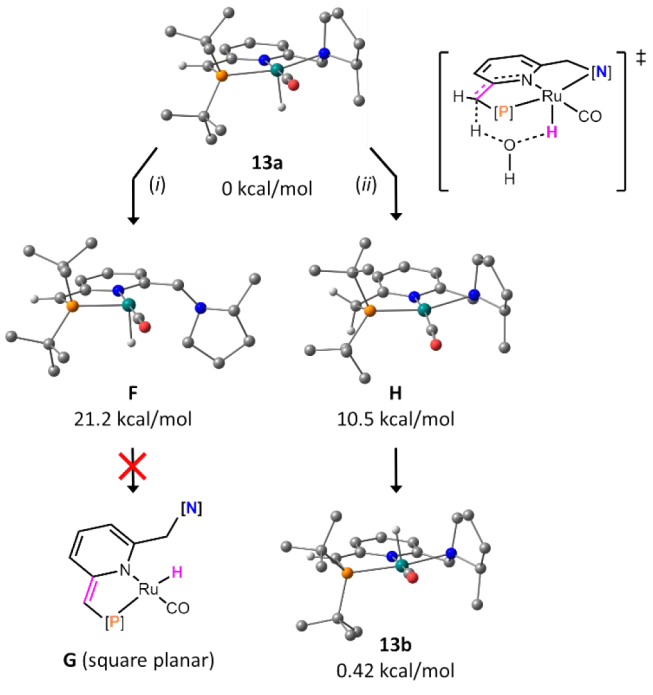

[a]Relative free energies are indicated.

https://dx.doi.org/10.1021/acs.organomet.9b00765
Organometallics 2020, 39, 544–555

as reference. The geometries were optimized in the gas phase at the TPSS/def2-TZVP level using dispersion corrections. Scheme 8 shows the structures of relevant stationary points on the potential energy surface and their relative Gibbs free energies (in kcal/mol). We initially focused on hydride migration by dissociation of the amine arm (path i). Detachment of the amine arm to generate a four-coordinate intermediate (**F**, Scheme 8) is uphill by 21.2 kcal/mol. Subsequent scans of the potential energy surface for migration of the Ru-bound hydride into the plane of the remaining ligands, however, show that this pathway is not feasible. Similarly, attempts to directly optimize the geometry of a planar, four-coordinate intermediate (species **G**, Scheme 8) resulted in a highly strained structure that is not energetically accessible (+42.7 kcal/mol, see the Supporting Information). Alternatively, transfer of the Ru-bound hydrogen atom to the ligand backbone (path ii) was explored, which results in the formation of a rearomatized 16-electron d^8 Ru(0) complex (**H**, Scheme 8). This species was calculated to have a Gibbs free energy of +10.5 kcal/mol with respect to the most stable isomer (**13a**), making this a plausible intermediate. The transition state of direct H transfer to the ligand, however, turned out to be high ($\Delta G^{\ddagger}$ = +41.6 kcal/mol relative to **13a**), not consistent with the mild reaction conditions under which Ru−H epimerization occurs experimentally.

We propose that this apparent dichotomy can be explained by the involvement of solvent molecules (and/or adventitious H_2O in the solvents) that can assist in this transformation: the conversion of **13a** to the Ru(0) species **H** is formally a H^+ transfer, which may be catalyzed by Lewis bases. In case of the related iridium complex (PNP)Ir(Ph) (P = P(*t*Bu)$_2$), a computational study showed that the presence of two H_2O molecules in the transition state results in a lowering of the reaction barrier by ca. 15 kcal/mol.[30] The role of proton shuttles in such reactions has been demonstrated to be quite general in metal−ligand cooperative systems.[31] We note that the qualitative difference observed experimentally for the rate of epimerization at the Ru center (vide supra: slower in benzene than in THF) is consistent with the notion that the more Lewis basic (and hygroscopic) solvent can facilitate H^+ transfer to the ligand backbone to generate the Ru(0) intermediate **H**.

Reaction of 13 with CO. The involvement of complex **H** that is implicated by the computational studies was further corroborated by the observation of Ru(0) species under a CO atmosphere. Treatment of the equilibrium mixture of **13a**,**b** (ratio 71:29) in benzene-d_6 with 1 atm of CO resulted in an immediate color change from dark red to greenish yellow. In the ^{1}H NMR spectrum the hydride signals of **13** (δ ∼−26 ppm) were replaced by two new Ru−H resonances at δ −4.74 and −5.07 ppm in a ratio that is identical with that of the starting material (**14a**:**14b** = 71:29). The new species have dearomatized pyridine rings (δ 6.6−5.3 ppm), indicating that these are the bis-carbonyl complexes **14a**,**b** (Scheme 9). The composition of the mixture slowly changes at room temperature: a **14a**:**14b** ratio of 34:66 is obtained after 1 week, and minor amounts (<5%) of two additional compounds with similar spectral features are present. The minor species are tentatively assigned to **14c**,**d**. When the reaction is carried out with pure isomer **13a**, the reaction mixture initially contains only a single isomer (**14a**). The ^{13}C NMR spectrum of **14a** confirms the presence of two carbonyl groups at δ 205.19 and 197.08 ppm. The IR spectrum of the **14a**−**d** mixture shows

Scheme 9. Reaction of 13 with CO to give Complexes 14 and 15[a]

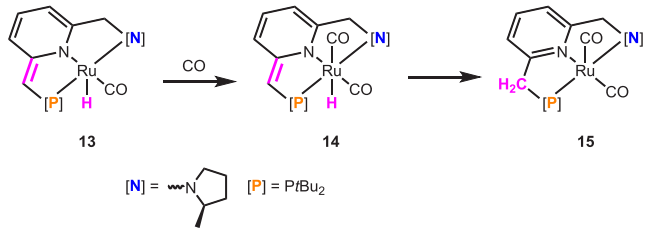

[a]Only diastereomers **13a**/**14a** (Ru_A) are shown for clarity, but an equilibrium mixture of diastereomers of **14** (and **15**) is obtained upon standing at room temperature

multiple intense bands in the region between 1873 and 2014 cm^{-1} that are assigned to CO stretching vibrations. In addition, the presence of a Ru−H fragment in **14** is supported by the presence of weaker bands around 2270 cm^{-1}. However, this also slowly equilibrates to a mixture containing **14a**,**b** as the major products.

In addition to establishment of equilibrium between diastereomers **14**, the appearance of an additional species with a rearomatized ligand backbone is observed (compound **15**). Conversely, no new Ru−H signals were observed for **15**, which indicates that rearomatization is the result of H transfer from Ru to the ligand. On this basis we formulate **15** as a (PNN)Ru^0 dicarbonyl complex (Scheme 9). After prolonged standing at room temperature (ca. 3 weeks), diastereomers of **15** are the only species in the solution, as indicated by the complete disappearance of Ru−H signals in the upfield range of the spectrum. The ^{31}P NMR spectrum shows that the two major products have signals at δ 80.1 and 79.9 ppm in a ratio of ca. 25:75. The ^{13}C NMR spectrum shows a single CO resonance at δ 208.3 ppm (J_{PC} = 2.4 Hz), which suggests that the carbonyl ligands rapidly exchange and thus that the stereochemistry at Ru is labile. IR spectroscopy of a sample of **15** prepared by drying a drop of the NMR solution on a KBr plate showed several new bands in the metal−carbonyl region, but also weak Ru−H absorptions. This may indicate that IR sample preparation (removal of CO atmosphere) partially converts **15** back to **14**. Although we were unable to unambiguously assign **15a**,**b**, the NMR data are consistent with diastereoisomeric Ru(0) dicarbonyls. Examples demonstrating migration of a metal hydride to the ligand backbone in related compounds have been reported,[32] and together with the reactivity of **13** toward CO described here, this supports the notion that Ru−H epimerization in these dearomatized pincer complexes occurs via Ru(0) intermediates.

Preliminary Catalysis Experiments. The complex **8** and the chiral derivatives **9** and **10** were tested as catalysts for oxa-Michael addition of benzyl alcohol to crotonitrile and *cis*-2-pentenenitrile (Scheme 10; see the Supporting Information for details). The precatalysts **8** and **9** were converted in situ to the active, dearomatized species **11** and **12** by treatment with 1 equiv of KO^{t}Bu. Catalysis with **13a** was carried out with isolated material. In all cases, 0.5 mol % of catalyst was treated with the solution of the unsaturated nitrile substrate and benzyl alcohol in THF, both at room temperature and at −30 °C. Reactions with either **11** or **13** were run for 17 h, after which the catalyst was quenched with air and the crude reaction mixture was analyzed by NMR spectroscopy (reactions with **11**) or purified by column chromatography (reactions with

https://dx.doi.org/10.1021/acs.organomet.9b00765
Organometallics 2020, 39, 544−555

Scheme 10. Catalytic Reactions Tested with Compounds 8–10/KO^{t}Bu or 13a

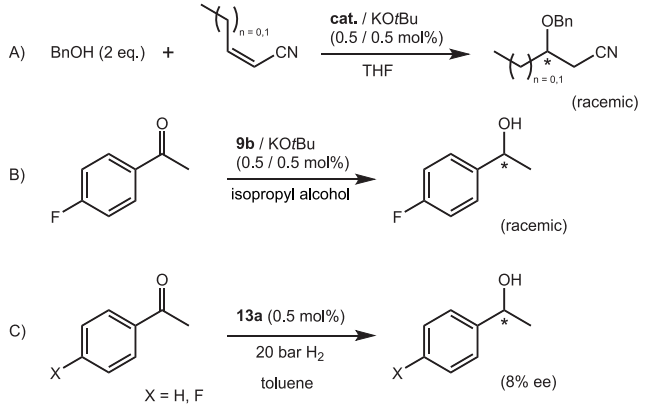

13). Both catalysts gave the desired oxa-Michael addition products, but chiral HPLC analysis indicated the products to be racemic in all cases. Catalytic reactions with **12** carried out under identical conditions were quenched after 5 (room temperature) or 30 min (−30 °C) reaction times, at which point only a few turnovers had occurred. Also for these reactions, no asymmetric induction was observed.

Transfer hydrogenation between 4-fluoroacetophenone and isopropyl alcohol with **9b**/KO^{t}Bu (0.5 mol %) was tested and shown to give 21% conversion to the corresponding benzyl alcohol after 16 h at 40 °C, but the product was racemic. However, room-temperature hydrogenation of acetophenone or 4-fluoroacetophenone with **13a** in toluene under 20 bar of H_2 gave full conversion to the alcohols, which were obtained with a low ee of 8%. It should be noted that moderate ee values were obtained in the transfer hydrogenation of acetophenone derivatives using Ru catalysts with P-chiral PNP or PCP ligands.[7c,33] Silica-supported metal complexes (Rh, Pd, Au, and Ru) with chiral CNN pincer ligands related to those reported here have been tested in the asymmetric hydrogenation of prochiral olefins, which gave high ee values only for the substrate diethyl 2-benzylidenesuccinate.[14]

A stoichiometric NMR experiment (C_6D_6) was carried out in which pure **13a** was treated with *cis*-2-pentenenitrile (2-PN). Although in the absence of substrate **13a** is stable in C_6D_6 solution for several hours, the addition of 2-pentenenitrile resulted in the immediate formation of a mixture of diastereomeric compounds. On the basis of the similarity of the NMR spectral features to those reported for the analogue with a NEt_2-substituted pincer arm,[11a] the main products were assigned as diastereomers of the metal–ligand cooperative nitrile activation products **16** (Scheme 11). The rapid formation of **16** as a diastereomeric mixture from pure **13a**/2-pentenenitrile shows that the substrate is able to effect racemization of the catalyst. The DFT-optimized geometries for the four different diastereomers of **16** were shown to have very similar Gibbs free energies (within 0.85 kcal/mol). Together, these data indicate that the stereochemistry in the active species **16** is labile and that under catalytically relevant conditions these compounds rapidly form diastereomeric mixtures, which precludes asymmetric induction with the present catalysts.

Scheme 11. Reaction of (PNN′)Ru(H)(CO) (13a) with 2-Pentenenitrile

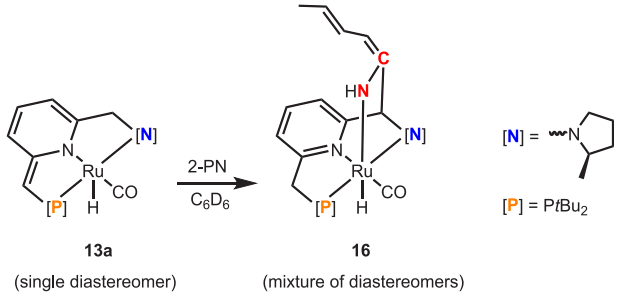

CONCLUSIONS

The incorporation of pyrrolidine substituents at the N arm of pyridine-based PNN pincer ligands was achieved. Both achiral and chiral derivatives were prepared, the latter by making use of enantiopure (*R*,*R*)-2,5-dimethylpyrolidine (with C_2 symmetry) and (*R*)-2-methylpyrrolidine (C_1). Synthesis of Milstein-type Ru complexes (PNN)Ru(H)(CO)(Cl) with these ligands allowed a study of the relative stability of diastereomers with different Ru- and N-centered stereochemistry. All possible diasteromers were observed in the crude reaction mixture, but crystallization for the (*R*,*R*)-2,5-dimethylpyrrolidine derivative **9** gave a single diasteromer, which was shown to be stable in solution; epimerization of the Ru stereocenter was not observed. When these compounds were converted to the dearomatized complexes (PNN′)Ru(H)(CO), the Ru stereocenter became labile at room temperature with the rate of epimerization being dependent on solvent polarity. The conversion of the dearomatized complex **13** to a Ru(0) derivative under a CO atmosphere, combined with computational data regarding the pathway for Ru–H epimerization, demonstrates that transfer of H from the Ru center to the ligand is likely responsible for the lack of stereochemical rigidity at Ru. Preliminary catalytic tests and stoichiometric experiments with an α,β-unsaturated nitrile substrate suggests that an equilibrium mixture of diastereomers is obtained under conditions relevant for oxa-Michael addition catalysis. Thus, the kinetic lability of the Ru stereocenter and the lack of a clear thermodynamic preference for one of the diastereoisomers do not allow reactions to occur with appreciable enantioselectivity with this class of catalysts. The results presented here provide useful insight into the dynamics of ruthenium hydride complexes with PNN ligands. Alternative ligand designs that do not rely on the Ru–H fragment as a means to induce enantiodiscrimination (e.g., C_2-symmetric PNP pincers) and replacement of the ruthenium-bound hydride with a less labile ligand are potential strategies that emerge from this work: research along those lines is currently in progress in our group.

EXPERIMENTAL SECTION

Synthesis of 8. In the glovebox, a Schlenk flask was loaded with ligand **4** (424 mg, 1.32 mmol, 1 equiv), $(PPh_3)_3Ru(Cl)(CO)H$ (1.26 g, 1.32 mmol, 1 equiv) and 20 mL of dry THF. Then the mixture was heated at 65 °C for 4 h, during which time the Ru precursor dissolved. After removal of the solvent, the residue was washed with dry diethyl ether (3 × 5 mL). The solid was dissolved in a minimal amount of THF and the solution filtered. The filtrate was layered with pentane for recrystallization or dried under vacuum, affording **8** as a light yellow solid product in 68% yield (437 mg, 0.90 mmol). ^{1}H NMR (400 MHz, acetone-d_6): δ/ppm 7.78 (t, J = 7.8 Hz, 1H, py-H4), 7.53 (d, J = 7.8 Hz, 1H, py-H3), 7.35 (d, J = 7.8 Hz, 1H, py-H5), 5.63 (d, J

https://dx.doi.org/10.1021/acs.organomet.9b00765
Organometallics 2020, 39, 544–555

= 14.5 Hz, 1H, py-6-CH_2N), 4.34 (t, J = 9.1 Hz, 1H, pyrr NCH_2CH$_2$), 3.76 (dd, J = 17.2, 9.9 Hz, 1H, py-2-CH_2P), 3.60 (d, J = 14.5 Hz, 1H, py-6-CH_2N), 3.36 (dd, J = 17.2, 8.5 Hz, 1H, py-2-CH_2P), 3.21 (t, J = 8.3 Hz, 1H, pyrr NCH_2CH$_2$), 2.58−2.46 (m, 1H, pyrr NCH_2CH$_2$), 2.45−2.29 (m, 2H, pyrr NCH_2CH_2), 2.27−2.11 (m, 1H, pyrr NCH$_2$CH_2), 1.93−1.80 (m, 2H, pyrr NCH$_2$CH_2), 1.35 (d, J = 13.0 Hz, 9H, P(C(CH_3)$_3$)$_2$), 1.32 (d, J = 13.0 Hz, 9H, P(C(CH_3)$_3$)$_2$), −15.43 (d, J = 27.3 Hz, 1H, Ru−H). ^{13}C NMR (101 MHz, acetone-d_6): δ/ppm 209.8 (CO), 162.9 (d, J = 4.0 Hz, py-C2), 161.2 (d, J = 1.9 Hz, py-C6), 138.3 (py-C4), 121.5 (d, J = 9.5 Hz, py-C3), 119.8 (py-C5), 68.0 (py-6-CH$_2$N), 67.2 (pyrr NCH$_2$CH$_2$), 59.7 and 59.7 (pyrr NCH$_2$CH$_2$), 38.16 (d, J = 12.8 Hz, py-2-CH$_2$P), 38.15 (d, J = 21.5 Hz, PC(CH$_3$)$_3$), 35.67 (d, J = 24.8 Hz, PC(CH$_3$)$_3$), 30.92 (d, J = 3.4 Hz, PC(CH$_3$)$_3$), 29.78 (d, J = 5.0 Hz, PC(CH$_3$)$_3$), 24.4 (pyrr NCH$_2$CH$_2$), 23.1 (pyrr NCH$_2$CH$_2$). ^{31}P NMR (162 MHz, acetone-d_6): δ/ppm 106.9. HRMS (ESI): calcd for $C_{20}H_{34}ClN_2OPRu$ [M − HCl + H$^+$] 451,14468, found 451,14497. IR (KBr): 1901 cm^{-1} (CO).

Synthesis of 9. Following a procedure analogous to that used for **8** gave compound **9** as a light yellow solid in 64% yield.

NMR data for pure **9b** (obtained by crystallization from acetone): ^{1}H NMR (400 MHz, acetone-d_6) δ/ppm 7.76 (t, J = 7.8, 1H, py-H4), 7.50 (d, J = 7.8 Hz, 1H, py-H3), 7.31 (d, J = 7.8 Hz, 1H, py-H5), 5.16 (d, J = 15.1 Hz, 1H, py-6-CH_2N), 3.96 (dd, J = 15.1, 2.9 Hz, 1H, py-6-CH_2N), 3.79−3.62 (m, 3H, py-2-CH_2Pand pyrr NCH (CH$_3$)CH$_2$), 3.43 (dd, J = 17.1, 8.8 Hz, 1H, py-2-CH_2P), 2.33−2.10 (m, 2H, pyrr NCH(CH$_3$)CH_2), 1.74−1.52 (m, 2H, pyrr NCH(CH$_3$)CH_2), 1.64 (d, J = 6.7 Hz, 3H, pyrr NCH(CH_3)CH$_2$), 1.36 (d, J = 13.1 Hz, 9H, PC(CH_3)$_3$), 1.34 (d, J = 13.1 Hz, 9H, PC(CH_3)$_3$), 0.99 (d, J = 6.8 Hz, 3H, pyrr NCH(CH_3)CH$_2$), −15.19 (d, J = 27.6 Hz, 1H, Ru−H); ^{13}C NMR (101 MHz, acetone-d_6) δ/ppm 209.4 (CO)*, 162.9 (d, J = 11.8 Hz, py-C2), 162.1 (py-C6), 138.4 (py-C4), 120.84 (d, J = 9.7 Hz, py-C3), 118.9 (py-C5), 67.0 and 66.2 (pyrr NCH(CH$_3$)CH$_2$), 61.6 (py-6-CH_2N), 38.0 and 37.8 (py-2-CH$_2$P), 30.7 (PC(CH$_3$)$_3$), 29.9 (pyrr NCH(CH$_3$)CH$_2$), 29.8 (PC(CH$_3$)$_3$), 29.7 (pyrr NCH-(CH$_3$)CH$_2$), 24.7 and 17.1 (pyrr NCH(CH$_3$)CH$_2$), loss of peak PC(CH$_3$)$_3$ for the intensity; ^{31}P NMR (162 MHz, acetone-d_6) δ/ppm 111.1. HRMS (ESI): calcd for $C_{22}H_{38}ClN_2OPRu$ [M − HCl + H$^+$] 479.17598, found 479.17670. An asterisk indicates a chemical shift taken from the gHMBC spectrum.

NMR data for isomer **9a**: ^{1}H NMR (400 MHz, acetone-d_6) δ/ppm 7.74 (t, J = 7.8 Hz, 1H, py-H4), 7.47 (d, J = 7.8 Hz, 1H, py-H3), 7.31 (d, J = 7.8 Hz, 1H, py-H5), 5.74 (d, J = 14.9 Hz, 1H, py-6-CH_2N), 5.32 (p, J = 7.5 Hz, 1H, pyrr NCH (CH$_3$)CH$_2$), 3.74 (dd, J = 17.1, 10.7 Hz, 1H, py-6-CH_2N), 3.72 (d, J = 14.9, 1H, py-2-CHP$_2$), 3.38 (dd, J = 17.1, 8.0 Hz, 1H, py-6-CHP$_2$), 2.95−2.80 (m, 1H, pyrr NCH(CH$_3$)CH$_2$), 2.58−2.40 (m, 1H, pyrr NCH(CH$_3$)CH_2), 2.03−1.87 (m, 1H, pyrr NCH(CH$_3$)CH_2), 1.85−1.72 (m, 1H, pyrr NCH(CH$_3$)CH_2), 1.36 (d, J = 13.1 Hz, 9H, PC(CH_3)$_3$), 1.34 (d, J = 13.1 Hz, 9H, PC(CH_3)$_3$), 1.27−1.15 (m, 2H, pyrr NCH(CH$_3$)-CH_2), 1.16 (d, J = 6.9 Hz, 3H, pyrr NCH(CH_3)CH$_2$), 0.91 (d, J = 6.2 Hz, 3H, pyrr NCH(CH_3)CH$_2$), −14.82 (d, J = 27.1 Hz, 1H, Ru−H); ^{31}P NMR (162 MHz, acetone-d_6) δ/ppm 109.1.

IR data for the **9a,b** mixture (KBr): 1906, 1883 cm^{-1} (CO).

Synthesis of 10. In the glovebox (PPh$_3$)$_3$Ru(Cl)(CO)H (654 mg, 0.687 mmol) was placed in a Schlenk flask, together with a solution of **6** (305 mg, 1.3 equiv of "crude") in 15 mL of dry THF. Outside of the glovebox the flask was heated in an oil bath (65 °C) overnight. The (PPh$_3$)$_3$Ru(Cl)(CO)H dissolved, and the solution became yellow. After it was cooled to room temperature, the solution was concentrated to about 3−4 mL, when a solid started coming from solution. The solid was filtered and washed with dry diethyl ether. After drying under vacuum a light yellow solid was obtained weighing 249 mg (0.50 mmol, 73%). ^{1}H NMR showed that all four possible isomers were present. Selected NMR data for the mixture: ^{1}H NMR (400 MHz, acetone-d_6) δ/ppm −14.90 (d, J = 26.8 Hz), −15.17 (d, J = 27.2 Hz), −15.43 (, J = 27.7 Hz, 0.86 H); ^{31}P NMR (162 MHz, acetone-d_6) δ/ppm 106.25 (d, J = 6.1 Hz), 105.72 (app s), 105.32 (app s), 104.84 (d, J = 7.10 Hz). NMR data for **10** crystallized from a concentrated acetone solution: ^{1}H NMR (400 MHz, THF-d_8) δ/ppm −14.71 (d, J = 26.6 Hz, 1.00 H), −14.95 (d, J = 27.1 Hz, 1.02 H), −15.16 (d, J = 27.6 Hz, 0.42 H), −15.25 (d, J = 27.5 Hz, 0.43 H); ^{31}P NMR (162 MHz, THF-d_8) δ 106.95, 106.45, 106.14, 105.56. Anal. Calcd for $C_{21}H_{36}ClN_2OPRu$: C, 50.44; H, 7.26; N, 5.60. Found: C, 49.98; H, 7.16; N, 5.53.

NMR-Scale Synthesis of 11. In the glovebox, complex **8** (9.4 mg, 0.02 mmol, 1 equiv) was placed in a small vial with 0.5 mL of d_8-THF, followed by the addition of tBuOK (2.3 mg, 0.02 mol, 1 equiv) at room temperature. After 5 min, the solution was transferred into a J. Young NMR tube and characterized by NMR. ^{1}H NMR (400 MHz, THF-d_8): δ/ppm 6.31 (ddd, J = 8.6, 6.4, 1.9 Hz, 1H, py-H4), 6.05 (d, J = 9.0 Hz, 1H, py-H3), 5.26 (d, J = 6.4 Hz, 1H, py-H5), 3.92 (d, J = 13.9 Hz, 1H, py-6-CH_2N), 3.52−3.44 (m, 1H, pyrr NCH_2CH$_2$), 3.44 (d, J = 13.9 Hz, 1H, py-6-CH_2N), 3.26 (d, J = 1.9 Hz, 1H, py-2-CHP), 2.80−2.66 (m, 2H, pyrr NCH_2CH$_2$), 2.49−2.39 (m, 1H, NCH$_2$CH_2), 2.36−2.27 (m, 1H, NCH_2CH$_2$), 2.26−2.16 (m, 1H, pyrr NCH$_2$CH_2), 2.03−1.91 (m, 2H, NCH$_2$CH_2), 1.26 (d, J = 12.7 Hz, 9H, PC(CH_3)$_3$), 1.18 (d, J = 13.3 Hz, 9H, PC(CH_3)$_3$), −25.78 (d, J = 25.8 Hz, 1H, Ru−H). ^{13}C NMR (101 MHz, THF-d_8): δ/ppm 208.1 (d, J = 12.9 Hz, CO), 169.90 (d, J = 16.6 Hz, py-C2), 157.2 (d, J = 2.4 Hz, py-C6), 132.5 (d, J = 1.8 Hz, py-C4), 114.3 (d, J = 17.2 Hz, py-C3), 96.4 (py-C5), 69.1 (py-6-CH$_2$N), 64.8 (NCH$_2$CH$_2$), 64.8 (d, J = 54.1 Hz, py-2-CHP), 57.2 (NCH$_2$CH$_2$), 38.7 (d, J = 25.0 Hz, PC(CH$_3$)$_3$), 35.9 (d, J = 27.5 Hz, PC(CH$_3$)$_3$), 29.6 (d, J = 4.4 Hz, PC(CH$_3$)$_3$), 29.49 (d, J = 4.5 Hz, PC(CH$_3$)$_3$), 24.7 and 24.5 (NCH$_2$CH$_2$). ^{31}P NMR (162 MHz, THF-d_8): δ/ppm 95.8.

NMR-Scale Synthesis of 12. In the glovebox, complex **9b** (10.3 mg, 0.02 mmol, 1 equiv) was placed in a small vial with 0.5 mL of d_6-benzene, followed by the addition of tBuOK (2.3 mg, 0.02 mol, 1 equiv) at room temperature. After all starting materials dissolved in the benzene, the solution was transferred into a J. Young NMR tube and characterized by NMR.

NMR data for **12b**: ^{1}H NMR (400 MHz, C$_6$D$_6$) δ/ppm 6.52 (t, J = 8.1 Hz, 1H, py-H4), 6.39 (d, J = 8.9 Hz, 1H, py-H5), 5.28 (d, J = 6.2 Hz, 1H, py-H3), 3.59−3.49 (m, 3H, py-6-CH_2N and py-2-CHP), 2.58−2.70 (t, J = 10.1 Hz, 2H), 2.34−2.21 (m, 1H), 1.61−1.54 (m, 1H), 1.51−1.43 (m, 1H), 1.41−1.35 (m, 18H, PC(CH_3)$_3$), 0.98 (dd, J = 11.2, 6.0 Hz, 1H), 0.63 (d, J = 6.7 Hz, 3H, pyrr NCH(CH_3)CH$_2$), 0.59 (d, J = 6.7 Hz, 3H, pyrr NCH(CH_3)CH$_2$), −26.46 (d, J = 25.9 Hz, 1H, Ru-H); ^{31}P NMR (162 MHz, C$_6$D$_6$) δ/ppm 94.65.

Characteristic NMR data for **12a**: ^{1}H NMR (400 MHz, C$_6$D$_6$) δ/ppm −25.38 (d, J = 26.2 Hz, 1H, Ru-H); ^{31}P NMR (162 MHz, C$_6$D$_6$) δ/ppm 97.3.

Synthesis of 13a. In the glovebox was weighed KOtBu (44 mg, 0.39 mmol, 1.12 equiv) in a 20 mL vial, to which was added 2 mL of THF. After the mixture had been cooled to −30 °C, a cold solution of **10** (174 mg, 0.348 mmol) in 9 mL of THF was added. The solution turned dark red almost instantly. The solution was placed in the freezer again and taken out several times to stir the mixture. After 3 h the solution was filtered through a 2 μm syringe filter and the filtrate was concentrated on the Schlenk line to ca. 0.5 mL. In the glovebox this was transferred to a 20 mL vial and the flask was rinsed with 0.5 mL of THF, which was also added. The solution was layered with 8 mL of pentane and placed in the freezer. This resulted in crystals suitable for single-crystal X-ray crystallography. After washing with pentane and drying under vacuum, **13a** was obtained as a dark crystalline solid weighing 82 mg (0.18 mmol, 51%). The mother liquor was reduced in volume and was layered with pentane to give a second crop, weighing 21 mg (0.045 mol, 13%). ^{1}H NMR (400 MHz, C$_6$D$_6$): δ/ppm 6.50 (ddd, J = 8.9, 6.9, 2.1 Hz, 1H, py-H4), 6.42 (d, J = 8.9 Hz, 1H, py-H5), 5.27 (d, J = 6.7 Hz, 1H, py-H3), 3.74 (d, J = 13.8 Hz, 1H, py-6-CH_2N), 3.57 (d, J = 2.1 Hz, 1H, py-2-CHP), 2.40 (dd, J = 13.8, 2.1 Hz, 1H, py-6-CH_2N), 2.12 (m, 1H, pyrr NCH_2CH$_2$), 2.03 (m, 1H, pyrr NCH(CH$_3$)CH_2), 1.79 (m, 1H, pyrr NCH(CH$_3$)CH$_2$, 1.69 (m, 1H, pyrr NCH$_2$CH_2), 1.54 (m, 1H, pyrr NCH_2CH$_2$), 1.49 (m, 1H, pyrr NCH(CH$_3$)CH_2), 1.36 (d, J = 10.2 Hz, 9H, PC(CH_3)$_3$), 1.33 (d, J = 10.9 Hz, 9H, PC(CH_3)$_3$), 1.15 (m, 1H, pyrr NCH$_2$CH_2), 1.11 (d, J = 6.1, 3H, NCH(CH_3)CH$_2$), −25.82 (d, J = 25.7, 1H, Ru-H). ^{13}C NMR (126 MHz, C$_6$D$_6$): δ/ppm 207.5 (d, J = 11.7 Hz, CO), 169.15 (d, J = 16.1 Hz, py-C4), 155.93

https://dx.doi.org/10.1021/acs.organomet.9b00765
Organometallics 2020, 39, 544−555

(d, J = 2.5 Hz, py-*C*2), 132.10 (s, py-*C*4), 114.23 (d, J = 17.6 Hz, py-*C*5), 96.24 (d, J = 3.2 Hz, py-*C*3), 66.89 (s, py-6-CH_2N), 65.31 (s, pyrr NC*H*(CH_3)CH_2), 64.92 (dd, J = 54.7, 1.6 Hz, py-2*C*HP), 54.69 (s, pyrr NCH$_2$*C*H$_2$), 38.01 (d, J = 26.5 Hz, P*C*(CH_3)$_3$), 35.21 (d, J = 27.7 Hz, PC(CH_3)$_3$), 31.78 (s, pyrr NCH(*C*H$_3$)CH$_2$), 29.12 (s, PC(*C*H$_3$)$_3$), 21.80 (s, pyrr NCH$_2$*C*H$_2$), 18.49 (s, pyrr NCH(*C*H$_3$)-*C*H$_2$). ^{31}P NMR (162 MHz, C_6D_6): δ/ppm 92.65. Anal. Calcd for $C_{21}H_{35}N_2OPRu$: C, 54.41; H, 7.61; N, 6.04. Found: C, 53.73; H, 7.76; N, 5.56. IR (KBr): 1891 cm^{-1} (CO).

NMR-Scale Synthesis of 14a. A J. Young NMR tube containing a solution of **13a** in 0.5 mL of C_6D_6 (5.5 mg, 0.024 M) was degassed by three freeze−pump−thaw cycles and backfilled with 1 bar of CO. An immediate color change from dark red to yellow took place when the tube was shaken. ^{1}H NMR (400 MHz, C_6D_6): δ/ppm 6.55 (t, J = 7.6 Hz, 1H, py-*H*4), 6.35 (d, J = 8.9 Hz, 1H, py-*H*5), 5.37 (d, J = 6.4 Hz, py-*H*3), 3.54 (d, J = 3.7 Hz, 1H, py-2-C*H*P), 3.54 (d, J = 14.0 Hz, 1H, py-6-C*H*$_2$N), 3.30 (t, J = 10.1 Hz, 1H, pyrr NC*H*$_2$CH$_2$), 2.91 (d, J = 14.2 Hz, 1H, py-6-C*H*$_2$N), 2.14 (qd, J = 9.6, 2.6 Hz, 1H, pyrr NC*H*$_2$CH$_2$), 1.77 (m, 1H, pyrr NCH$_2$C*H*$_2$), 1.54 (m, 2H, one of pyrr NCH(CH_3)C*H*$_2$ and pyrr NC*H* (CH_3)CH_2 overlapping), 1.43 (d, J = 13.5 Hz, 9H, PC(*C*H$_3$)$_3$), 1.34 (d, J = 13.4 Hz, 9H, PC(*C*H$_3$)$_3$), 1.28 (m, 1H, pyrr NCH(CH$_3$)C*H*$_2$), 1.18 (m, 1H, pyrr NCH$_2$C*H*$_2$), 1.11 (d, J = 5.5 Hz, 3H, pyrr NCH(*C*H$_3$)CH$_2$), −4.74 (d, J = 23.3 Hz, 1H, Ru-*H*). ^{13}C NMR (101 MHz, C_6D_6): δ/ppm 205.19 (d, J = 11.8 Hz, CO), 197.08 (s, CO), 168.04 (d, J = 13.9 Hz, py-*C*6), 155.14 (s, py-*C*2), 131.89 (d, J = 1.9 Hz, py-*C*4), 113.18 (d, J = 17.2 Hz, py-*C*5), 97.15 (s, py-*C*3), 69.97 (s, py-6-CH_2N), 69.56 (s, pyrr NCH(CH$_3$)-CH$_2$), 66.25 (s, pyrr NCH$_2$CH$_2$), 62.63 (d, J = 58.1 Hz, pyr-2-*C*HP), 37.91 (d, J = 22.2 Hz, P*C*(CH_3)$_3$), 36.98 (d, J = 30.8 Hz, P*C*(CH_3)$_3$), 30.86 (d, J = 3.4 Hz, PC(CH_3)$_3$), 30.78 (s, pyrr NCH(CH_3)CH_2), 30.19 (d, J = 4.5 Hz, PC(CH_3)$_3$), 20.89 (s, pyrr NCH$_2$*C*H$_2$), 18.95 (s, pyrr NCH(CH_3)*C*H$_2$). ^{31}P NMR (162 MHz, C_6D_6): δ/ppm 96.95 (d, J = 2.2 Hz). IR data for the mixture of isomers (KBr): 1873−2014 cm^{-1} (CO).

NMR-Scale Synthesis of 15. A J. Young NMR tube containing an equilibrated mixture of isomers **13a**,**b** (ratio 71:29) in 0.5 mL of C_6D_6 (4.0 mg, 0.022 M) was degassed by three freeze−pump−thaw cycles and backfilled with 1 bar of CO. An immediate color change from dark red to yellow took place when the tube was shaken. Over a period of 1 month the color changed to greenish yellow. The product mixture consists of three different isomers of **15** in a 27:68:5 ratio on the basis of ^{31}P NMR integration. Major species: ^{1}H NMR (400 MHz, C_6D_6) δ/ppm 7.35 (d, J = 7.9 Hz, 1H, py-*H*3), 7.20 (t, J = 7.7 Hz, 1H, py-*H*4), 7.06 (d, J = 7.7 Hz, 1H, py-*H*5), 4.15 (d, J = 14.4 Hz, 1H, py-6-C*H*$_2$N), 3.45 (d, J = 14.4 Hz, 1H, py-6-C*H*$_2$N), 3.18 (d, J = 10.0 Hz, 1H, py-2-C*H*$_2$P), 3.15 (d, J = 10.0 Hz, 1H, py-2-C*H*$_2$P), 3.01 (dt, J = 8.7, 3.0 Hz, 1H, pyrr NC*H*$_2$CH$_2$), 2.36 (m, 1H, pyrr NC*H* (CH_3)CH_2), 2.12 (q, J = 8.7 Hz, 1H, pyrr NC*H*$_2$CH$_2$), 1.75 (m, 1H, NCH(CH_3)C*H*$_2$), 1.63 (m, 1H, pyrr NCH$_2$C*H*$_2$), 1.48 (m, 1H, pyrr NCH$_2$C*H*$_2$), 1.34 (m, 1H, pyrr NCH(CH_3)C*H*$_2$), 1.20 (d, J = 4.1 Hz, 9H, PC(CH_3)$_3$), 1.16 (d, J = 4.0 Hz, 9H, PC(*C*H$_3$)$_3$), 1.08 (d, J = 5.9 Hz, 3H, pyrr NCH(*C*H$_3$)CH$_2$); ^{13}C NMR (101 MHz, C_6D_6) δ/ppm 208.33 (d, J = 2.4 Hz, CO), 160.68 (d, J = 1.8 Hz py-*C*2), 155.90 (d, J = 2.0 Hz, py-*C*6), 136.57 (d, J = 2.0 Hz, py-*C*4), 124.36 (d, J = 4.1 Hz, py-*C*5), 120.99 (d, J = 2.5 Hz, py-*C*3), 60.24 (s, py-6-CH_2N), 59.95 (s, pyrr NCH(CH_3)CH_2), 54.71 (s, pyrr NCH$_2$CH$_2$), 37.68 (d, J = 4.6 Hz, P*C*(CH_3)$_3$), 37.55 (d, J = 4.8 Hz, P*C*(CH_3)$_3$), 34.52 (d, J = 10.9 Hz, pyr-*C*H$_2$P), 33.26 (s, pyrr NCH(CH_3)*C*H$_2$), 30.15 (d, J = 4.7 Hz, PC(CH_3)$_3$), 30.07 (d, J = 4.7 Hz, PC(*C*H$_3$)$_3$), 22.31 (s, pyrr NCH$_2$CH$_2$), 19.57 (s, pyrr NCH(*C*H$_3$)CH$_2$); ^{31}P NMR (162 MHz, C_6D_6) δ/ppm 79.91 (s).

X-ray Crystallography. Single crystals of compounds **7**, **8**, **9b**, **10**, and **13a** were mounted on top of a cryoloop and transferred into the cold nitrogen stream (100 K) of a Bruker-AXS D8 Venture diffractometer. Data collection and reduction were done using the Bruker software suite APEX3.[34] The final unit cell was obtained from the *xyz* centroids of 9903 (**7**), 9716 (**8**), 9193 (**9b**), 9682 (**10**), and 9883 (**13a**) reflections after integration. A multiscan absorption correction was applied, on the basis of the intensities of symmetry-related reflections measured at different angular settings (SADABS).[34] The structures were solved by direct methods using SHELXT,[35] and refinement of the structure was performed using SHELXL.[36] The hydrogen atoms were generated by geometrical considerations, constrained to idealized geometries, and allowed to ride on their carrier atoms with an isotropic displacement parameter related to the equivalent displacement parameter of their carrier atoms. For **8**, refinement indicated the presence of disordered solvent, the contribution of which was removed using the PLATON/SQUEEZE routine.[37] For **10**, the structure was initially solved in space group $P2_1/n$, which resulted in a highly disordered pyrrolidine ring. Solving the structure in space group $P2_1$ allowed refinement of two independent molecules: one of these molecules was well-defined, whereas the other still showed disorder in the pyrrolidine ring. From the refinement, two orientations of the pyrrolidine ring were identified in this molecule, which differed in the chirality at N. A two-site occupancy model was applied for this disordered part, which converged on an equal sof (0.5) for both disorder components. The well-defined pyrrolidine ring in the first molecule was used to restrain the refinement of the disordered part using the SAME instruction. Some atoms in the disordered fragment showed unrealistic displacement parameters, and RIGU/SIMU instructions were applied. For the chiral structures, the handedness of the model was chosen on the basis of refinement of Flack's parameter;[20] all molecules have the expected carbon-centered chirality (from the pyrrolidine stereocenter). Crystal data and details of data collection and refinement are presented in Table S1.

■ ASSOCIATED CONTENT

Supporting Information

The Supporting Information is available free of charge at https://pubs.acs.org/doi/10.1021/acs.organomet.9b00765.

Cartesian coordinates for the calculated structures (XYZ)

Full experimental and characterization details and computational data (PDF)

Accession Codes

CCDC 1964354−1964358 contain the supplementary crystallographic data for this paper. These data can be obtained free of charge via www.ccdc.cam.ac.uk/data_request/cif, or by emailing data_request@ccdc.cam.ac.uk, or by contacting The Cambridge Crystallographic Data Centre, 12 Union Road, Cambridge CB2 1EZ, UK; fax: +44 1223 336033.

■ AUTHOR INFORMATION

Corresponding Authors

Johannes G. de Vries − *Leibniz Institute für Katalyse e.V., Universität Rostock, 18059 Rostock, Germany;* orcid.org/0000-0001-5245-7748; Email: johannes.devries@catalysis.de

Edwin Otten − *Stratingh Institute for Chemistry, University of Groningen, 9747 AG Groningen, The Netherlands;* orcid.org/0000-0002-5905-5108; Email: edwin.otten@rug.nl

Authors

Johan Bootsma − *Stratingh Institute for Chemistry, University of Groningen, 9747 AG Groningen, The Netherlands*

Beibei Guo − *Stratingh Institute for Chemistry, University of Groningen, 9747 AG Groningen, The Netherlands*

Complete contact information is available at: https://pubs.acs.org/10.1021/acs.organomet.9b00765

Notes

The authors declare no competing financial interest.

https://dx.doi.org/10.1021/acs.organomet.9b00765
Organometallics 2020, 39, 544−555

■ ACKNOWLEDGMENTS

Financial support from The Netherlands Organisation for Scientific Research (NWO) (VIDI grant to E.O.) and the China Scholarship Council (grant to B.G.) is gratefully acknowledged. We thank the Center for Information Technology of the University of Groningen for their support and for providing access to the Peregrine high-performance computing cluster.

■ REFERENCES

(1) (a) Van Koten, G.; Gossage, R. A. *The privileged pincer-metal platform: Coordination chemistry & applications*; Springer: 2015; Vol. *54*. (b) Morales-Morales, D. *Pincer Compounds: Chemistry and Applications*; Elsevier: 2018. (c) Peris, E.; Crabtree, R. H. Key factors in pincer ligand design. *Chem. Soc. Rev.* **2018**, *47*, 1959.

(2) Liu, J.-K.; Gong, J.-F.; Song, M.-P. Chiral palladium pincer complexes for asymmetric catalytic reactions. *Org. Biomol. Chem.* **2019**, *17*, 6069.

(3) (a) Ito, J.-i.; Nishiyama, H. In *Pincer Compounds*; Morales-Morales, D., Ed.; Elsevier: 2018; p 1. (b) Gong, J.-F.; Zhu, X.; Song, M.-P. In *Pincer Compounds*; Morales-Morales, D., Ed.; Elsevier: 2018; p 191. (c) Hyodo, K.; Nakamura, S. In *Pincer Compounds*; Morales-Morales, D., Ed.; Elsevier: 2018; p 219.

(4) (a) Bedford, R. B.; Chang, Y.-N.; Haddow, M. F.; McMullin, C. L. Tuning ligand structure in chiral bis(phosphite) and mixed phosphite−phosphinite PCP-palladium pincer complexes. *Dalton Transactions* **2011**, *40*, 9034. (b) Baber, R. A.; Bedford, R. B.; Betham, M.; Blake, M. E.; Coles, S. J.; Haddow, M. F.; Hursthouse, M. B.; Orpen, A. G.; Pilarski, L. T.; Pringle, P. G.; Wingad, R. L. Chiral palladium bis(phosphite) PCP-pincer complexes via ligand C−H activation. *Chem. Commun.* **2006**, 3880.

(5) Gibbons, S. K.; Xu, Z.; Hughes, R. P.; Glueck, D. S.; Rheingold, A. L. Chiral Bis(Phospholane) PCP Pincer Complexes: Synthesis, Structure, and Nickel-Catalyzed Asymmetric Phosphine Alkylation. *Organometallics* **2018**, *37*, 2159.

(6) (a) Gosiewska, S.; Herreras Martinez, S.; Lutz, M.; Spek, A. L.; van Koten, G.; Klein Gebbink, R. J. M. Diastereopure Cationic NCN-Pincer Palladium Complexes with Square Planar η4-N, C, N, O Coordination. *Eur. J. Inorg. Chem.* **2006**, *2006*, 4600. (b) Gosiewska, S.; Huis in't Veld, M.; de Pater, J. J. M.; Bruijnincx, P. C. A.; Lutz, M.; Spek, A. L.; van Koten, G.; Klein Gebbink, R. J. M. Novel enantiopure non-C2-symmetric NCN-pincer palladium complexes with l-proline chiral auxiliaries: mer η3-N, C, N versus square planar η4-N, C, N, O coordination. *Tetrahedron: Asymmetry* **2006**, *17*, 674.

(7) (a) Williams, B. S.; Dani, P.; Lutz, M.; Spek, A. L.; van Koten, G. Development of the First P-Stereogenic PCP Pincer Ligands, Their Metallation by Palladium and Platinum, and Preliminary Catalysis. *Helv. Chim. Acta* **2001**, *84*, 3519. (b) Morales-Morales, D.; Cramer, R. E.; Jensen, C. M. Enantioselective synthesis of platinum group metal complexes with the chiral PCP pincer ligand R, R-{C_6H_4-2,6-($CH_2P^*Ph^tBu)_2$}. The crystal structure of R, R-PdCl{C_6H_3-2,6-($CH_2P^*Ph^tBu)_2$}. *J. Organomet. Chem.* **2002**, *654*, 44. (c) Arenas, I.; Boutureira, O.; Matheu, M. I.; Díaz, Y.; Castillón, S. Synthesis of a P-Stereogenic PNPtBu, Ph Ruthenium Pincer Complex and Its Application in Asymmetric Reduction of Ketones. *Eur. J. Org. Chem.* **2015**, *2015*, 3666. (d) Huber, R.; Passera, A.; Mezzetti, A. Iron(II)-Catalyzed Hydrogenation of Acetophenone with a Chiral, Pyridine-Based PNP Pincer Ligand: Support for an Outer-Sphere Mechanism. *Organometallics* **2018**, *37*, 396.

(8) (a) Gorla, F.; Togni, A.; Venanzi, L. M.; Albinati, A.; Lianza, F. Synthesis of an Optically Active Platinum(II) Complex Containing a New Terdentate P-C-P Ligand and Its Catalytic Activity in the Asymmetric Aldol Reaction of Methyl Isocyanoacetate. X-ray Crystal Structure of [2,6-Bis[(1′S,2′S)-1′-(diphenylphosphino)-2′,3′-O-isopropylidene-2′,3′-dihydroxypropyl]phenyl](.eta.1-nitrato)platinum-(II). *Organometallics* **1994**, *13*, 1607. (b) Longmire, J. M.; Zhang, X. Synthesis of chiral phosphine ligands with aromatic backbones and their applications in asymmetric catalysis. *Tetrahedron Lett.* **1997**, *38*, 1725. (c) Feng, J.-J.; Chen, X.-F.; Shi, M.; Duan, W.-L. Palladium-Catalyzed Asymmetric Addition of Diarylphosphines to Enones toward the Synthesis of Chiral Phosphines. *J. Am. Chem. Soc.* **2010**, *132*, 5562.

(9) (a) Gunanathan, C.; Milstein, D. In *Bifunctional Molecular Catalysis*; Ikariya, T., Shibasaki, M., Eds.; Springer: Berlin Heidelberg, 2011; Vol. *37*, p 55. (b) Gunanathan, C.; Milstein, D. Applications of Acceptorless Dehydrogenation and Related Transformations in Chemical Synthesis. *Science* **2013**, *341*, 1229712. (c) Khusnutdinova, J. R.; Milstein, D. Metal−Ligand Cooperation. *Angew. Chem., Int. Ed.* **2015**, *54*, 12236.

(10) Eijsink, L. E.; Perdriau, S. C. P.; de Vries, J. G.; Otten, E. Metal−ligand cooperative activation of nitriles by a ruthenium complex with a de-aromatized PNN pincer ligand. *Dalton Trans.* **2016**, *45*, 16033.

(11) (a) Perdriau, S.; Zijlstra, D. S.; Heeres, H. J.; de Vries, J. G.; Otten, E. A Metal−Ligand Cooperative Pathway for Intermolecular Oxa-Michael Additions to Unsaturated Nitriles. *Angew. Chem., Int. Ed.* **2015**, *54*, 4236. (b) Guo, B.; Zijlstra, D. S.; de Vries, J. G.; Otten, E. Oxa-Michael Addition to α,β-Unsaturated Nitriles: An Expedient Route to γ-Amino Alcohols and Derivatives. *ChemCatChem* **2018**, *10*, 2868.

(12) Tang, S.; Milstein, D. Template catalysis by manganese pincer complexes: oxa- and aza-Michael additions to unsaturated nitriles. *Chem. Sci.* **2019**, *10*, 8990.

(13) Guo, B.; de Vries, J. G.; Otten, E. Hydration of Nitriles using a Metal-Ligand Cooperative Ruthenium Pincer Catalyst. *Chem. Sci.* **2019**, *10*, 10647.

(14) (a) Boronat, M.; Corma, A.; González-Arellano, C.; Iglesias, M.; Sánchez, F. Synthesis of Electron-Rich CNN-Pincer Complexes, with N-Heterocyclic Carbene and (S)-Proline Moieties and Application to Asymmetric Hydrogenation. *Organometallics* **2010**, *29*, 134. (b) Del Pozo, C.; Corma, A.; Iglesias, M.; Sánchez, F. Immobilization of (NHC)NN-Pincer Complexes on Mesoporous MCM-41 Support. *Organometallics* **2010**, *29*, 4491. (c) Del Pozo, C.; Corma, A.; Iglesias, M.; Sánchez, F. Recyclable mesoporous silica-supported chiral ruthenium-(NHC)NN-pincer catalysts for asymmetric reactions. *Green Chem.* **2011**, *13*, 2471.

(15) Zhang, L.; Tang, Y.; Han, Z.; Ding, K. Lutidine-Based Chiral Pincer Manganese Catalysts for Enantioselective Hydrogenation of Ketones. *Angew. Chem., Int. Ed.* **2019**, *58*, 4973.

(16) Short, R. P.; Kennedy, R. M.; Masamune, S. An improved synthesis of (−)-(2R,5R)-2,5-dimethylpyrrolidine. *J. Org. Chem.* **1989**, *54*, 1755.

(17) Zhao, D.; Kuethe, J. T.; Journet, M.; Peng, Z.; Humphrey, G. R. Efficient and Practical Synthesis of (R)-2-Methylpyrrolidine. *J. Org. Chem.* **2006**, *71*, 4336.

(18) Zhang, J.; Leitus, G.; Ben-David, Y.; Milstein, D. Facile Conversion of Alcohols into Esters and Dihydrogen Catalyzed by New Ruthenium Complexes. *J. Am. Chem. Soc.* **2005**, *127*, 10840.

(19) (a) Gargir, M.; Ben-David, Y.; Leitus, G.; Diskin-Posner, Y.; Shimon, L. J. W.; Milstein, D. PNS-Type Ruthenium Pincer Complexes. *Organometallics* **2012**, *31*, 6207. (b) Tang, Z.; Otten, E.; Reek, J. N. H.; van der Vlugt, J. I.; de Bruin, B. Dynamic Ligand Reactivity in a Rhodium Pincer Complex. *Chem. - Eur. J.* **2015**, *21*, 12683.

(20) Flack, H. D.; Bernardinelli, G. Absolute structure and absolute configuration. *Acta Crystallogr., Sect. A: Found. Crystallogr.* **1999**, *55*, 908.

(21) Li, W.; Xie, J.-H.; Lin, H.; Zhou, Q.-L. Highly efficient hydrogenation of biomass-derived levulinic acid to γ-valerolactone catalyzed by iridium pincer complexes. *Green Chem.* **2012**, *14*, 2388.

(22) Connelly, N. G.; Hartshorn, R. M.; Damhus, T.; Hutton, A. T. *Nomenclature of inorganic chemistry: IUPAC recommendations 2005*; Royal Society of Chemistry: 2005.

(23) Flack, H. D. Chiral and Achiral Crystal Structures. *Helv. Chim. Acta* **2003**, *86*, 905.

https://dx.doi.org/10.1021/acs.organomet.9b00765
Organometallics 2020, 39, 544−555

(24) Zhang, J.; Leitus, G.; Ben-David, Y.; Milstein, D. Efficient Homogeneous Catalytic Hydrogenation of Esters to Alcohols. *Angew. Chem., Int. Ed.* **2006**, *45*, 1113.
(25) Vogt, M.; Nerush, A.; Iron, M. A.; Leitus, G.; Diskin-Posner, Y.; Shimon, L. J. W.; Ben-David, Y.; Milstein, D. Activation of Nitriles by Metal Ligand Cooperation. Reversible Formation of Ketimido- and Enamido-Rhenium PNP Pincer Complexes and Relevance to Catalytic Design. *J. Am. Chem. Soc.* **2013**, *135*, 17004.
(26) Tao, J.; Perdew, J. P.; Staroverov, V. N.; Scuseria, G. E. Climbing the Density Functional Ladder: Nonempirical Meta–Generalized Gradient Approximation Designed for Molecules and Solids. *Phys. Rev. Lett.* **2003**, *91*, 146401.
(27) Weigend, F.; Ahlrichs, R. Balanced basis sets of split valence, triple zeta valence and quadruple zeta valence quality for H to Rn: Design and assessment of accuracy. *Phys. Chem. Chem. Phys.* **2005**, *7*, 3297.
(28) Grimme, S.; Antony, J.; Ehrlich, S.; Krieg, H. A consistent and accurate ab initio parametrization of density functional dispersion correction (DFT-D) for the 94 elements H-Pu. *J. Chem. Phys.* **2010**, *132*, 154104.
(29) Oki, M.; Ohira, M. Dynamic NMR Study on Rates of Dissociation of an Amine Ligand in an Organometallic Compound. *Chem. Lett.* **1982**, *11*, 1267.
(30) Iron, M. A.; Ben-Ari, E.; Cohen, R.; Milstein, D. Metal-ligand cooperation in the trans addition of dihydrogen to a pincer Ir(I) complex: a DFT study. *Dalton Trans.* **2009**, 9433.
(31) (a) Prokopchuk, D. E.; Tsui, B. T. H.; Lough, A. J.; Morris, R. H. Intramolecular C-H/O-H Bond Cleavage with Water and Alcohol Using a Phosphine-Free Ruthenium Carbene NCN Pincer Complex. *Chem. - Eur. J.* **2014**, *20*, 16960. (b) Qu, S.; Dang, Y.; Song, C.; Wen, M.; Huang, K.-W.; Wang, Z.-X. Catalytic Mechanisms of Direct Pyrrole Synthesis via Dehydrogenative Coupling Mediated by PNP-Ir or PNN-Ru Pincer Complexes: Crucial Role of Proton-Transfer Shuttles in the PNP-Ir System. *J. Am. Chem. Soc.* **2014**, *136*, 4974. (c) Nerush, A.; Vogt, M.; Gellrich, U.; Leitus, G.; Ben-David, Y.; Milstein, D. Template Catalysis by Metal−Ligand Cooperation. C−C Bond Formation via Conjugate Addition of Non-activated Nitriles under Mild, Base-free Conditions Catalyzed by a Manganese Pincer Complex. *J. Am. Chem. Soc.* **2016**, *138*, 6985. (d) Smith, N. E.; Bernskoetter, W. H.; Hazari, N. The Role of Proton Shuttles in the Reversible Activation of Hydrogen via Metal−Ligand Cooperation. *J. Am. Chem. Soc.* **2019**, *141*, 17350.
(32) (a) Barrios-Francisco, R.; Balaraman, E.; Diskin-Posner, Y.; Leitus, G.; Shimon, L. J. W.; Milstein, D. PNN Ruthenium Pincer Complexes Based on Phosphinated 2,2′-Dipyridinemethane and 2,2′-Oxobispyridine. Metal−Ligand Cooperation in Cyclometalation and Catalysis. *Organometallics* **2013**, *32*, 2973. (b) Oren, D.; Diskin-Posner, Y.; Avram, L.; Feller, M.; Milstein, D. Metal−Ligand Cooperation as Key in Formation of Dearomatized NiII−H Pincer Complexes and in Their Reactivity toward CO and CO2. *Organometallics* **2018**, *37*, 2217.
(33) Medici, S.; Gagliardo, M.; Williams, S. B.; Chase, P. A.; Gladiali, S.; Lutz, M.; Spek, A. L.; van Klink, G. P. M.; van Koten, G. Novel P-Stereogenic PCP Pincer-Aryl Ruthenium(II) Complexes and Their Use in the Asymmetric Hydrogen Transfer Reaction of Acetophenone. *Helv. Chim. Acta* **2005**, *88*, 694.
(34) Bruker. *APEX3, SAINT and SADABS*; Bruker AXS Inc., Madison, WI, USA, 2016.
(35) Sheldrick, G. SHELXT - Integrated space-group and crystal-structure determination. *Acta Crystallogr., Sect. A: Found. Adv.* **2015**, *71*, 3.
(36) Sheldrick, G. Crystal structure refinement with SHELXL. *Acta Crystallogr., Sect. C: Struct. Chem.* **2015**, *71*, 3.
(37) Spek, A. PLATON SQUEEZE: a tool for the calculation of the disordered solvent contribution to the calculated structure factors. *Acta Crystallogr., Sect. C: Struct. Chem.* **2015**, *71*, 9.

https://dx.doi.org/10.1021/acs.organomet.9b00765
Organometallics 2020, 39, 544−555